Available online at www.sciencedirect.com
SCIENCE DIRECT®
Biochemical and Biophysical Research Communications 305 (2003) 79–86
BBRC
www.elsevier.com/locate/ybbrc

Single-molecule detection of efflux pump machinery in *Pseudomonas aeruginosa*

Xiao-Hong Nancy Xu,* William Brownlow, Shuang Huang, and Jun Chen

Department of Chemistry and Biochemistry, Old Dominion University, Norfolk, VA 23529, USA

Received 1 April 2003

Abstract

Real-time single-molecule microscopy and spectroscopy were used to monitor single molecules moving in and out of live bacterial cells, *Pseudomonas aeruginosa*. Ethidium bromide (EtBr) was chosen as the fluorescence probe because it emitted a weak fluorescence in aqueous solution (outside of the cells) and became strongly fluorescent as it entered the cells and intercalated with DNA. Such changes in fluorescence intensity by individual EtBr molecules were measured to determine the influx and efflux rates of EtBr by the cells. The transport rates for EtBr through the energized extrusion pumps of these strains (WT, nalB-1, and ΔABM) of *P. aeruginosa* were measured and showed stochastic behavior with the average being (2.86 ± 0.12), (2.80 ± 0.13), and $(2.74 \pm 0.39)\,s^{-1}$, respectively. The transport rates of the three strains were independent of substrate concentration at the single-molecule level. In contrast to bulk (many molecules) measurements, single-molecule detection allowed the influx and efflux kinetics to be observed in low substrate concentrations at the molecular level.

Keywords: Efflux pump; Ethidium bromide; Multi-drug resistance; Membrane transport; *Pseudomonas aeruginosa*; Single-molecule detection; Fluorescence microscopy and spectroscopy; Single live cell imaging

All living organisms appear equipped with an effective means to defend themselves against the hazards of noxious compounds (e.g., hydrophobic materials, heavy metals, cytotoxic agents, and drugs) by lowering the intracellular concentration of such compounds through active extrusion [1–3]. It is of great interest and importance to study the mechanism of such universally occurring extrusion pump machinery. *Pseudomonas aeruginosa* is a ubiquitous Gram-negative bacterium and has emerged to be the leading cause of nosocomial infections in cancer, transplantation, burn, and cystic fibrosis patients. These infections are impossible to eradicate in part because of the bacterial intrinsic resistance to a wide spectrum of structurally and functionally unrelated antibiotics [3–6]. Several efflux systems, including MexAB-OprM, MexCD-OprJ, MexEF-OprN, and MexXY-OprM, have been reported in *P. aeruginosa* [6–9]. The MexAB-OprM pump is the major efflux pump in wild-type (WT) cells. This pump consists of two inner membrane proteins (MexA and MexB) and one outer membrane protein (OprM) [8,9]. The MexB protein consists of 1046 amino acid residues and is assumed to extrude the xenobiotics utilizing the proton motive force as the energy source [6,7]. Studies showed that the inner membrane subunits appeared to specify the substrates to be transported [8,9]. Several models have been proposed in an attempt to describe the possible mechanism of the pump [8–13]. Time-course fluorescence spectroscopy has been used as a popular tool for real-time monitoring of the substrates accumulated in bulk bacterial cells [14]. Such bulk measurements have significantly advanced the understanding of efflux machinery in both prokaryotes and eukaryotes [3,14]. However, these bulk measurements showed the accumulated kinetics of substrates in the cells and represented the average behavior of a massive number of pumps in cells. To study the influx (passive diffusion

* Corresponding author. Fax: 1-757-683-4628.
E-mail address: xhxu@odu.edu (X.-H. Nancy Xu).
URL: www.odu.edu/sci/xu/xu.htm.

0006-291X/03/$ - see front matter © 2003 Elsevier Science (USA). All rights reserved.
doi:10.1016/S0006-291X(03)00692-2

into the cell) and efflux kinetics of substrates at the molecular level, single-molecule detection (SMD) was introduced in this study.

SMD is a way to study and characterize physical and chemical properties of individual molecules in detail [15–17]. This approach allows one to look beyond the ensemble average and provides a new opportunity to study the pump machinery at the molecular level. A variety of approaches were recently demonstrated for SMD in solution and several excellent review articles have been published [15–17]. Studies of SM diffusion in phospholipid membrane [18] and free solution [19–23] have been demonstrated. Detection of single-molecules labeled with fluorophores in single living cells [24] and on cellular membrane [25], and single-molecule analysis of chemotactics signaling in living cells [26] have also been reported. However, direct monitoring of influx and efflux of a single molecule through intact cell membrane remains unexplored. The key challenges of such endeavor include (i) how to detect a single molecule outside and inside a living cell and distinguish the difference between them; (ii) how to develop a sufficient rapid mean to follow the molecule while it is passing through the living cellular membrane, and (iii) how to select the biocompatible molecules that will not perturb the cellular function.

In this work, we demonstrated the possibility of real-time measurement of membrane pump machinery of single living cells at the single-molecule level. MexAB-OprM membrane pump in WT of *P. aeruginosa* was used as a working model and the pump efficiency of single EtBr molecules transported by WT and its mutants was investigated using single-molecule fluorescence microscopy and spectroscopy.

Materials and methods

Chemicals and supplies

Quartz slides (25×75 mm), coverslips ($22 \times 30 \times 0.08$ mm), and Nuclepore membrane (25 mm diameter with 6 μm thickness) were purchased from VWR, Edmund Scientific and Corning Corporation, respectively. Ultra-pure water (Nanopore, 18 MΩ, sterilized) and PBS buffer solutions were illuminated under a UV-lamp (Labconco) for 48 h to photo-bleach fluorescence contaminant and triple filtered using a 0.22 μm sterilized membrane filter (Costar) before they were used to prepare solutions for SMD. EtBr (Sigma) solution was prepared in ultra-pure bleaching water and triple filtered using 0.2 μm sterilized membrane filters prior to being incubated with cells. All other reagents, Na_3PO_4, Na_2HPO_4, NaH_2PO_4, and NaCl, were purchased from Sigma and used without further purification or treatment.

Cell culture and preparation

Pseudomonas aeruginosa cell lines [9,27,28], PAO4290 (a wild-type level expression), nalB-1 (TNP030#1, MexAB-OprM over expression mutant), and ΔABM (TNP076, MexAB-OprM deficient mutant), were used. Cells were grown in L-broth medium containing 1% tryptone, 0.5% yeast extract, and 0.5% NaCl at pH 7.2 while rotating at 120 rpm and 37 °C. Cells were first pre-cultured to ensure a full growth and then cultured for an additional 8 h. Cells were harvested by centrifugation at 7500 rpm and 23 °C for 10 min, washed three times with 50 mM phosphate buffer (pH 7.0), and then suspended again in the same buffer ($A_{600\,nm} = 0.1$). The cell solution (20× dilution of $A_{600\,nm} = 0.1$) was used for SMD of pump machinery in single living cells.

Bulk measurement using fluorescence spectroscopy

Time courses of fluorescence intensity of EtBr at 590 ± 10 nm from 3.0 mL cell solutions containing 40 and 0.010 μM EtBr were directly recorded by a fluorescence spectrometer (Perkin–Elmer LS50B), using a time-drive mode with a 3 s data acquisition interval and 488 ± 10 nm excitation (Fig. 1). Time courses of fluorescence intensity of each type of cells in a particular concentration of EtBr were recorded on the same day. The experiment was repeated at least three times using fresh cell solutions.

Single-molecule and single-cell microscopy and spectroscopy

Instrumentation. The entire system included a 6 μm thickness thin-layer microchannel, an inverted microscope (Zeiss Axiovert 100/135D)

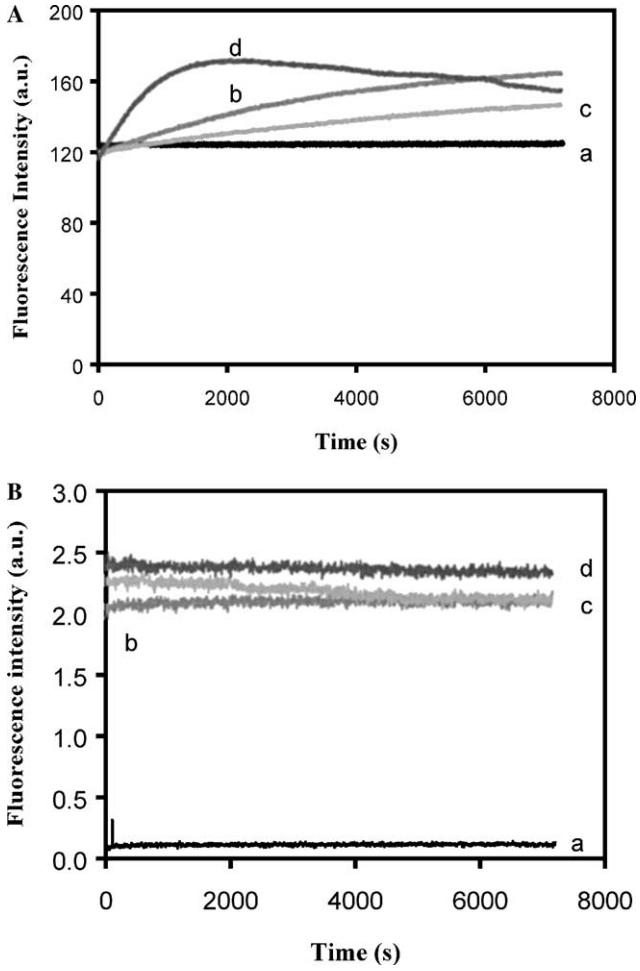

Fig. 1. Study of concentration dependence of accumulation kinetics in intact cells of *P. aeruginosa*: time courses of fluorescence intensity of EtBr at 590 ± 10 nm (a) in the PBS buffer and in the presence of intact cells of *P. aeruginosa*, (b) WT, (c) nalB-1, and (d) ΔABM, acquired directly from a 3.0 mL cell solution containing (A) 40 μM and (B) 0.010 μM (10 nM) EtBr using fluorescence spectroscopy with a time-drive mode at a 3 s data acquisition interval and 488 ± 10 nm excitation.

with an 100× microscope objective (ultrafluar, numerical aperture = 1.2, Zeiss), a detector (a 512 × 512 pixel ICCD, Princeton Instruments, Intensified PentaMAX-512 EFT at 5 MHz with Gen II high-resolution image intensifier), a microscope illuminator (halogen lamp, 100 W) with an oil dark-field condenser (Oil 1.43–1.20, Nikon) for dark-field microscopy, and the unfocused filtered Ar^+ laser beam at 514.5 nm (Spectra-physics, Beam Lok 2045-15/4) for total-internal reflection fluorescence microscopy (Fig. 2). The ICCD element was maintained at −25 °C by a thermoelectric cooler. A band-pass interference filter at 600 nm with FWHM of 40 nm (Coherent) was used to collect the fluorescence signal. The entire imaging system, including a microscope and ICCD camera, was placed in the dark box and all measurements were made in a darkened room to reduce the ambient light.

Procedure. A rectangle hole (~$12 \times 16\,mm^2$) was made on the center of a Nuclepore membrane (6 μm thickness), which was placed on the surface of a cleaned quartz slide and rapidly sealed around the membrane using glue (Duco cement) to create a microwell. The cell solution (20× dilution of $A_{600\,nm} = 0.1$) was mixed with EtBr, while a timer was started to record the time. The 30 μL of cell solution containing 0.2 and 0.4 nM EtBr was added on the center of the microwell. A coverslip was added on the top of the well and sealed to create the microchannel. The microchannel was placed on the microscope stage with the coverslip facing downward to the 100× objective. The slide was secured onto the microscope stage using the tape to eliminate perturbation movement. The immersion oil (ultrafluora, Zeiss) was added onto the slide surface. The dark field condenser attached to the illuminated lamp of the inverted microscope using a homemade adaptor was then brought in contact with the immersion oil on the slide surface. Single living cells were imaged using the dark-field optical microscopy to identify the location of a single cell (Fig. 2A). The size of the sub-frame was then selected to contain the observation zone for single EtBr in a single cell (solid-line square) and in the solution (absence of cell, dash-line square). The dark-field condenser was carefully lifted from the slide surface and microscope illuminator (halogen lamp, 100 W) was turned off.

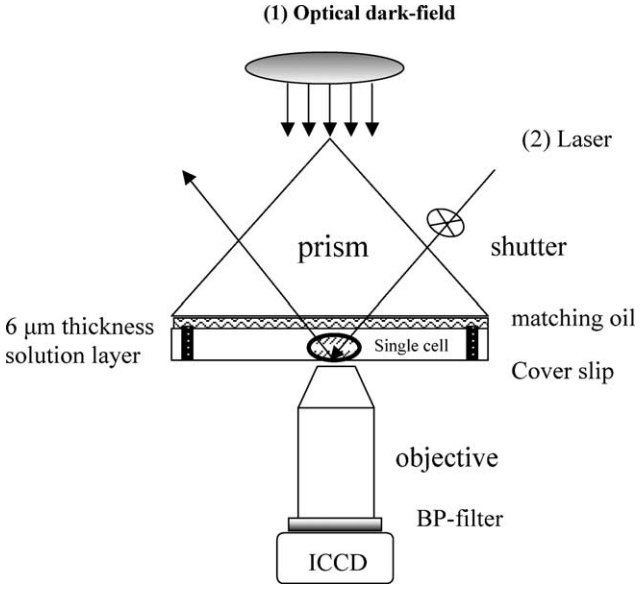

Fig. 2. Schematic diagram of single-cell and single-molecule microscopy and spectroscopy: (1) dark-field optical microscopy for imaging and locating of single living bacterial cells, *P. aeruginosa* and (2) thin-layer total-internal reflection fluorescence microscopy for detection of single molecules in and out of single living cells. Both microscopes shared the same inverted microscope, microscope objective, and ICCD detector. Dark-field microcopy used halogen lamp (100 W) as an illumination source, whereas the thin-layer total-internal reflection microscopy used the unfocused filtered Ar^+ laser beam at 514.5 nm as the excitation source. The laser penetrated the solution before being totally reflected at the interface of the coverslip and air. This configuration provided a lower background than epifluorescence arrangement. A mechanical shutter placed in front of the laser beam was synchronized with ICCD shutter to limit the exposure of the sample to the laser and to prevent the sample from photobleaching. Exposure time of ICCD and shuttle delay time were monitored using an oscilloscope to ensure the precise measurement of temporal resolution.

A fused-silica right-angle prism was then placed on the quartz slide with the index matching oil (ultrafluora, Zeiss) sandwiched between them. The unfocused filtered Ar^+ laser beam at 514.5 nm was directed into the fused-silica right-angle prism via fiber-optic. The laser penetrated the solution before being totally reflected at the interface of the coverslip and air. This provided a total-internal reflection configuration to avoid excitation source from penetrating into the ICCD detector and hence reduce background. A mechanical shutter (Melles Griot, CA) placed in front of the laser beam was synchronized with ICCD shutter to limit exposure of the sample to the laser and to prevent the sample from photobleaching. The power of laser beam directed to the prism was measured before and after the experiments using a power meter (broadband power/energy meter 13PEM001, Melles Griot). Fluorescence was detected by the ICCD that was mounted at the bottom entrance of the microscope, facing upward. Two hundred sequence images of single living cells in 0.2 and 0.4 nM EtBr were acquired with 70 ms temporal resolution and 99.84 exposure time. Fifteen–seventeen sets of such sequence images were measured during 80 min to provide 15–17 snapshots of influx and efflux kinetics. After fluorescence measurements, the prism was then gently removed from the slide surface and replaced by the dark-field condenser. Dark-field optical microscopy was applied to image the cells and to confirm the position of the cells that remained unchanged through the entire experiment. The experiment was repeated at least 3 times and 3–10 cells of each strain were investigated.

Results and discussion

Study of pump machinery using bulk fluorescence spectroscopic measurements

Time courses of fluorescence intensity of 40 and 0.01 μM EtBr in the cell solutions of WT, nalB-1, and ΔABM (Fig. 1) were measured at 590 ± 10 nm to follow the accumulation kinetics of EtBr in the cells. The fluorescence intensity of EtBr in the buffer solution remained almost unchanged over time demonstrating the photostability of EtBr. This suggested that the change of fluorescence intensity in cell solution could be used to follow the accumulation of EtBr in cells. The result clearly showed that time courses of fluorescence intensity of EtBr depended on substrate (EtBr) concentrations. As substrate concentration decreased, the distinguished extrusion kinetics in three strains decreased.

In 40 μM EtBr, the fluorescence intensity of EtBr in all three strains increased with time, indicating the accumulation of EtBr in cells (Fig. 1A). The fluorescence intensity of ΔABM (mutant devoid of MexAB-OprM) and nalB-1 (mutant with over-expression pump)

increased with time most and least rapidly, respectively. This result suggested that nalB-1 extruded EtBr out of cells much more effectively than WT and ΔABM because of the over expression of pump proteins. On the contrary, ΔABM was unable to extrude EtBr using MexAB-OprM and thus accumulated EtBr more rapidly than WT and nalB-1. Unlike those observed in 40 μM EtBr, time courses of the fluorescence intensity in 0.010 μM EtBr for all three strains showed the similarity that the fluorescence intensity remained almost unchanged over time (Fig. 1B). This result suggested that no detectable change of fluorescence intensity was observed by fluorescence spectrometer. In order to probe the pump machinery in the low substrate concentration, we developed and applied single-molecule fluorescence microscopy and spectroscopy to measure the influx and efflux kinetics of EtBr in live cells.

Sizes of single living cells as SM detection volume

To detect single substrate molecules (EtBr), we used sizes of single living cells as individual detection volume and thin-layer total-internal reflection fluorescence microscopy to eliminate the excitation noise and increase the signal-to-noise ratio. High-resolution optical images of WT of *P. aeruginosa* were acquired using optical dark-field microscopy, indicating that the sizes of optical images of cells were around 2 μm in length, 0.5 μm in width and in height (Fig. 3). Similar results for ΔABM and nalB-1 were also observed. The sizes of cells were confirmed by transmission electron microscope (TEM). Thus, the detection volume of a single cell was 5×10^{-16} L. Cell concentration (20× dilution of $A_{600\,nm} = 0.1$) and 0.2–0.4 nM EtBr were used to ensure statistically a single cell with about a single EtBr molecule or less.

We identified the location of a single cell in the solution using dark-field optical microscopy, selected the subframe that contained a single cell (solid-line square) (Fig. 3), and then acquired sequence fluorescence images using SM fluorescence microscopy and spectroscopy. Integrated fluorescence intensity of a detection zone in the part of the image, including a single cell (solid-line square) and the other part of the image excluding the cell (solution only, dash-line square) was measured in the same solution using the same laser power and recorded in the same frame. The former served as a signal for monitoring of the influx and efflux of a single EtBr molecule by a single living cell. The latter offered the real-time measurement of a single EtBr molecule in the solution that served as a reference and background for the signal measurement. The subtracted fluorescence intensity of the latter from the former represented a single EtBr molecule in or out of a single living cell. Using this novel approach, the fluctuation of ICCD dark noise, laser beam, buffer solution, and photodecomposition of EtBr molecules, was reduced to the minimum because the fluorescence intensity of EtBr in and out of the cell was measured simultaneously in the same frame from the same solution at the same laser power. This allowed us to distinguish single molecules in and out of single living cells and measure influx and efflux kinetics at the molecular level.

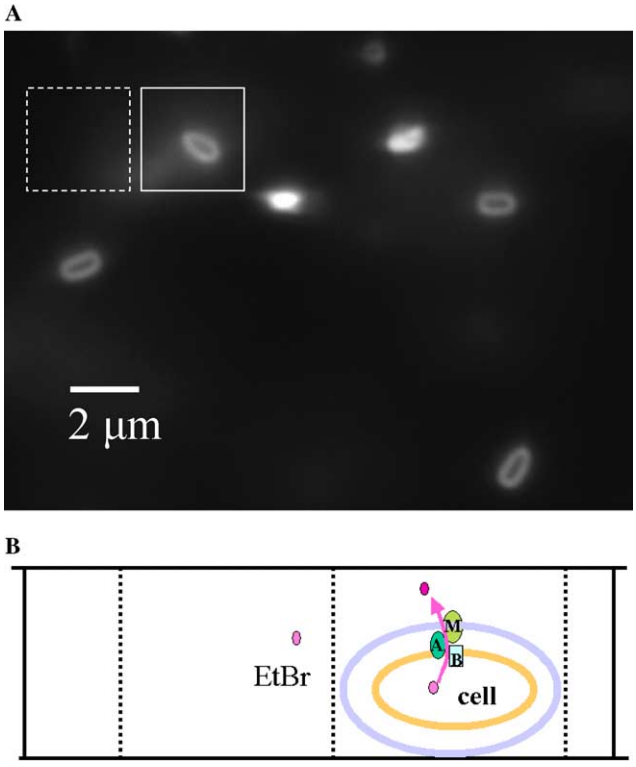

Fig. 3. (A) Sub-frame high-resolution optical image of single living bacterial cells, *P. aeruginosa* (WT), acquired using dark-field microscopy showing the well-dispersed single cells in the microchannel. Solid-line and dash-line squares represented the selected pixel area for integrated fluorescence intensity analysis of EtBr in a single cell and in solution, respectively. (B) Schematic illustration of the selected detection volume, including a single EtBr molecule in the solution (left) and with a single living cell (right) in the microchannel. EtBr entered the cell using passive diffusion and was extruded out of the cell by MexAB-OprM.

Membrane pump efficiency of WT

Two hundred sequence images of WT cells in 0.2 nM EtBr were recorded using ICCD with 70 ms temporal resolution and 99.84 ms exposure time. Seventeen sets of such sequence images recorded over 80 min showed snap shots of influx and efflux of a single EtBr by a single WT cell. We selected an area (13 × 13 pixel) that contained an individual cell (solid-line square) and an equal sized pixel area that contained no cells (solution only) (dash-line square) in the same frame (Fig. 3A). We then analyzed the integrated fluorescence intensity of each area and subtracted the integrated intensity of area (dash-line square) where no cell was present (EtBr in solution) from that of the area where a cell was present (solid-line

square) (EtBr in a single cell). Representative plots of subtracted integrated fluorescence intensity versus time Fig. 4A clearly demonstrated that the change of fluorescence intensity of a single EtBr molecule with a single WT cell was above the fluctuation of background emission of a single cell and ICCD noise (baseline). Unlike eukaryote cells, the auto-fluorescence of WT was not observed. This might be attributable to its tiny size ($2 \times 0.5 \times 0.5\,\mu m$).

As EtBr molecules entered the cell and intercalated with DNA, the fluorescence intensity of a single EtBr molecule in the cell increased over the intensity of EtBr in solution. Thus, the subtracted integrated intensity became positive. On the contrary, as EtBr molecules were transported out of the cell, the fluorescence intensity of a single cell decreased below the intensity of EtBr in solution. Thus, the subtracted integrated intensity became negative. EtBr concentration in solution was higher than in a live cell. Thus, the molecule must be extruded out of the cell through the active efflux mechanism. Taken together, the subtracted fluorescence intensity was positive or negative representing the location of a single EtBr molecule, in or out of a single living cell,

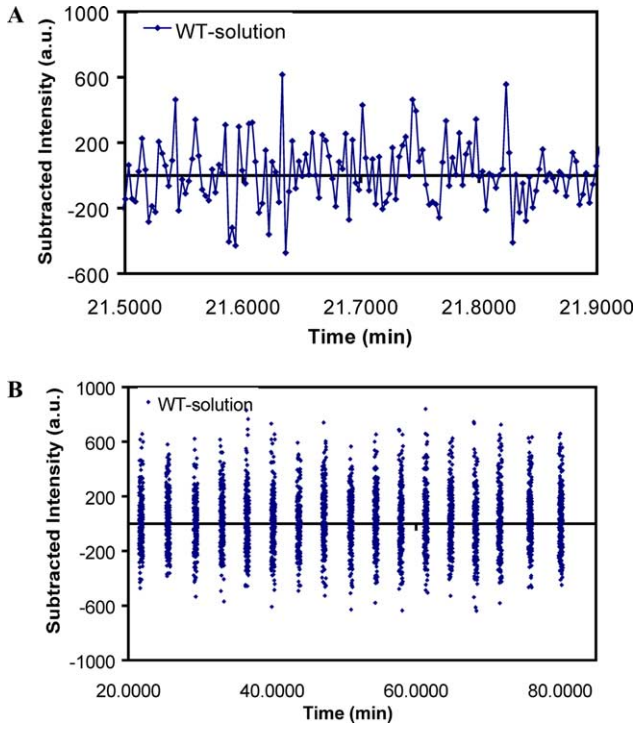

Fig. 4. Representative plots of (A) subtracted integrated fluorescence intensity of a single EtBr molecule in solution (dash-line square) from that in a single living cell (WT) (solid-line square) versus time (min) at 21.5000–21.9000 min; (B) 17 sets of the 200 consecutive images were taken during 80 min. A zoom-in display of (B) at 21.5000–21.9000 min was shown in (A). The selected analyzed zone (dash-line and solid-line square) was 13×13 pixel in the same frame (167×127-pixel). Every set of 200 sequence images was taken with a 70 ms temporal resolution and 99.84 ms CCD exposure time.

respectively. The frequency of changed sign of the subtracted fluorescence intensity from negative to positive or from positive to negative represented the rates of influx and efflux of a single EtBr molecule by a single living cell, respectively. Seventeen sets of 200 sequence images recorded in Fig. 4 demonstrated that the stochastic influx and efflux rate of a single EtBr molecule with the average at $(2.86 \pm 0.12)\,s^{-1}$. The average of influx and efflux rates remained nearly constant over time. This was in an excellent agreement with the bulk measurement of accumulated EtBr in WT cells (Fig. 1B).

To determine whether EtBr entered the cells or stayed on the membrane, the fluorescence intensity of the membrane on live cells incubated with 0.1 nM to 400 μM EtBr was measured. The result showed insignificant change of fluorescence intensity of EtBr on membrane [29]. This result suggested that the increasing fluorescence intensity in Fig. 4 was attributable to EtBr entering the cell. To investigate whether the photodecomposition lifetime of EtBr affected the influx and efflux rate measurement, we changed the laser power from 2.6 to 1.3 mW and performed the same measurement. The results are similar to those in Fig. 4 with the average pump efficiency within $(2.86 \pm 0.12)\ s^{-1}$, which suggested that photodecomposition did not significantly interfere the influx and efflux measurements at 1.3–2.6 mW.

Temporal resolution and concentration dependence

In order to determine whether influx and efflux rates depended on the temporal resolutions of SM measurements, the rates in a single WT containing 0.2 nM EtBr were measured in both 70 and 60 ms temporal resolution using the similar approach. Plots of the subtracted intensity versus time were similar to those in Fig. 4 showing the stochastic behavior with the average influx and efflux rates approaching constant over time. On average, the pump efficiency was within $(2.86 \pm 0.12)\ s^{-1}$. These data suggested that it took more than 10 ms for a single EtBr molecule to pass through the membrane of living WT cell in 0.2 nM because the average efflux pump efficiency remained the same for both measurements with 70 and 60 ms resolution.

To study whether single membrane pump efficiency depended upon EtBr concentrations within SM regime, the rates in a single WT containing 0.4 nM EtBr were measured. This concentration still ensured statistically one molecule with one cell. Plots of subtracted integrated intensity versus time were similar to the one in Fig. 4 showing the stochastic behavior with the average influx and efflux rates being approximately constant over time. On average, the pump efficiency was within $(2.86 \pm 0.12)\,s^{-1}$. This result suggested that we indeed monitored the influx and efflux rates at the single-molecule level because the pump efficiency was independent

on substrate concentration only at the single-molecule level and was dependent on substrate concentration at the multi-molecule level [29,30].

Mutant dependence

To determine whether influx and efflux kinetics in such low EtBr concentration depended upon mutants of WT, two mutants of PAO4290 (a wild-type level expression), nalB-1 (TNP030#1, MexAB-OprM over expression mutant), and ΔABM (TNP076, MexAB-OprM deficient mutant), were used [9,27,28]. Representative plots of subtracted integrated fluorescence intensity of EtBr molecules with a single nalB-1 cell versus time were shown in Fig. 5. The rate of influx and efflux of a single EtBr molecule by a single living nalB-1 cell showed the stochastic behavior with the average pump efficiency at $(2.80 \pm 0.13)\,s^{-1}$. This appeared similar to the pump efficiency of WT in the presence of same EtBr concentration (0.2 nM). This result suggested that the influx and efflux rates of a single substrate molecule (EtBr) were independent on number of pumps expressed per cell. This was consistent with unique feature of single-molecule measurements.

Using similar approaches, the influx and efflux rates of ΔABM in 0.2 nM EtBr were measured. Representative plots of subtracted integrated fluorescence intensity of a single ΔABM in 0.2 nM EtBr versus time were shown in Fig. 6. The rates of influx and efflux of a single EtBr molecule by a single ΔABM cell showed the stochastic behavior with the average pump efficiency at $(2.74 \pm 0.39)\,s^{-1}$, which was only slightly smaller than that of nalB-1 and WT. Because there were other pump proteins (e.g., MexCD-OprJ) with the low expression level in ΔABM, the observation of efflux in ΔABM might be attributable to these pump proteins. The detection of efflux in ΔABM also suggested that other types of active extrusion pumps might function in ΔABM mutant. This result is correlated with our recent measurements of efflux kinetics in ΔABM [30,31]. In these experiments, we observed astonishing efflux of EtBr by ΔABM in high concentrations of EtBr (100–400 μM) [30]. This new finding is also supported by the genome data, which indicated that chromosome of *P. aeruginosa* encodes more than dozen of unidentified efflux pump proteins [32]. This result also showed the unique capability of SMD for study of efflux machinery and transportation mechanism in live cells at the single-molecule level.

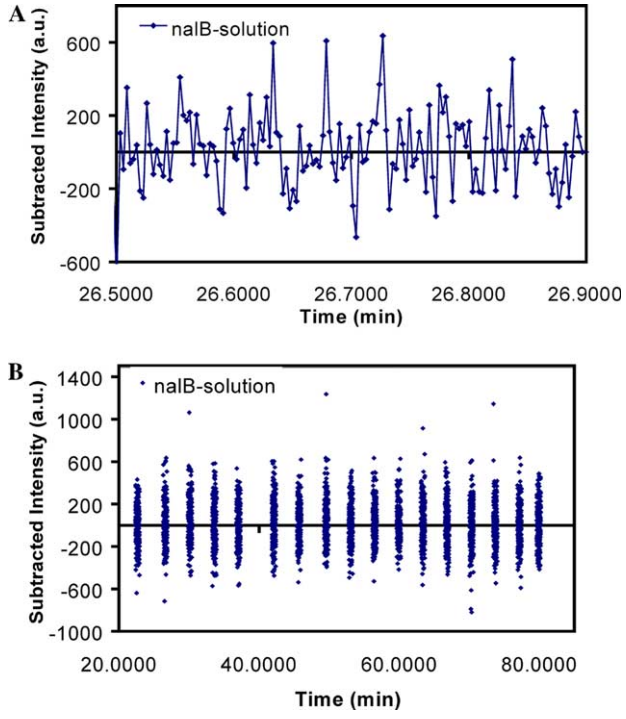

Fig. 5. Representative plots of (A) subtracted integrated fluorescence intensity of a single EtBr molecule in solution (dash-line square) from that in a single living cell (nalB-1) (solid-line square) versus time (min) at 26.5000–26.9000 min; (B) 17 sets of the 200 consecutive pictures were taken during 80 min. A zoom-in display of (B) at 26.5000–26.9000 min was shown in (A). The selected analyzed zone (dash-line and solid-line square) was 13 × 13 pixel in the same frame (136 × 109 pixel). The temporal resolution and data analysis were the same as those in Fig. 4.

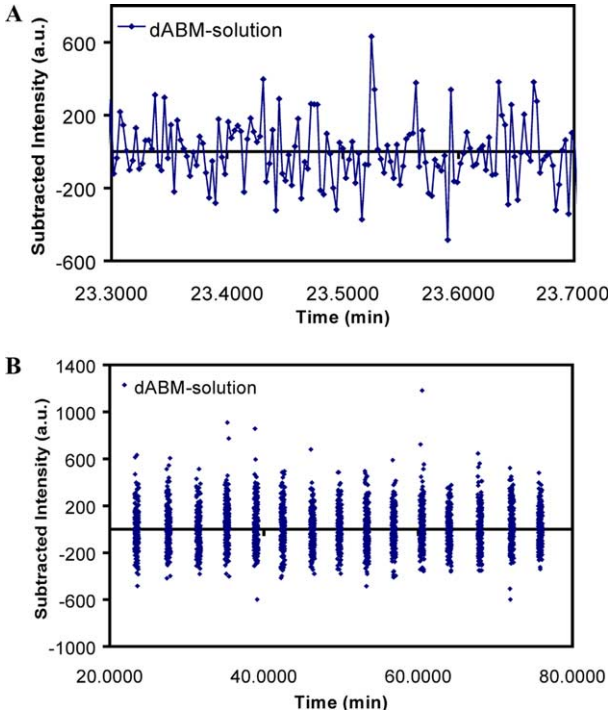

Fig. 6. Representative plots of (A) subtracted integrated fluorescence intensity of a single EtBr molecule in solution (dash-line square) from that in a single living cell (ΔABM) (solid-line square) versus time (min) at 23.3000–23.7000 min; (B) 15 sets of the 200 consecutive pictures were taken during 80 min. A zoom-in display of (B) at 23.3000–23.7000 min was shown in (A). The selected analyzed zone (dash-line and solid-line square) was 13 × 13 pixel in the same frame (160 × 146 pixel). The temporal resolution and data analysis were the same as those in Fig. 4.

Likewise, the influx and efflux rates of nalB-1 and ΔABM were measured in 0.2–0.4 nM EtBr, at 1.3–2.6 mW laser power and 60–70 ms temporal resolution. The results suggested the independence of concentrations within 0.2–0.4 nM, the laser power of 1.3–2.6 mW, and the temporal resolution of 60–70 ms. The data suggested that the transport rate of a single EtBr molecule through the membrane of live nalB-1 and ΔABM cells appeared to be greater than 10 ms, similar to those observed in WT. The average of influx and efflux rates in live nalB-1 and ΔABM cells remained nearly constant over time (Figs. 5 and 6), which was in excellent agreement with those measured using bulk analysis (Fig. 1B).

Conclusion

We presented a new platform for real-time detection and observation of single molecules passing through living cell membrane. This was demonstrated by measurement of the transport rates of a single EtBr molecule through single living bacterial cells, *P. aeruginosa*, using SM fluorescence microscopy and spectroscopy. The results suggested that the transport rates at the SM level were independent of substrate concentration and the expression levels of pump proteins. One can now use this approach to study other transport mechanisms at the SM level and to probe other membrane pumps for the better understanding of the universal extrusion cell defense mechanism.

Acknowledgments

We thank Taiji Nakae (Tokai University School of Medicine, Japan) and Hiroshi Yoneyama (Tohoku University, Japan) for three strains of *Pseudomonas aeruginosa* and helpful discussion. The support of this work in part by NIH (RR15057-01), Old Dominion University, in the form of start-up and Dominion Scholar Fellowship (Huang), is gratefully acknowledged.

References

[1] S.P. Cole, G. Bhardwaj, J.H. Gerlach, J.E. Mackie, C.E. Grant, K.C. Almquist, A.J. Stewart, E.U. Kurz, A.M. Duncan, R.G. Deeley, Overxpression of a transporter gene in a mutidrug-resistant human lung cancer cell line, Science 258 (1992) 1650–1654.

[2] M.F. Rosenberg, Q. Mao, A. Holzenburg, R.C. Ford, R.G. Deeley, S.P. Cole, The structure of the multidrug resistance protein 1 (MRP1/ABCC1) crystallization and single-particle analysis, J. Biol. Chem. 276 (2001) 16076–16082.

[3] (For review:) B.M. Byan, T.J. Dougherty, D. Beaulieu, J. Chuang, B.A. Dougherty, J.F. Barrett, Efflux in bacteria: what do we really know about it?, Expert Opin. 10 (7) (2001) 1409–1422, and reference therein.

[4] K. Poole, Multidrug efflux pumps and antimicrobial resistance in *Pseudomonas aeruginosa* and related organisms, J. Mol. Microbiol. Biotechnol. 3 (2) (2001) 255–264.

[5] T. Nakae, Multiantibiotic resistance caused by active drug extrusion in *Pseudomonas aeruginosa* and other gram-negative bacteria, Microbiologia 13 (3) (1997) 273–284, and reference therein.

[6] D. Ma, D.N. Cook, J.E. Hearst, H. Nikaido, Efflux pumps and drug resistance in gram-negative bacteria, Trends Microbiol. 2 (12) (1994) 489–493.

[7] N. Masuda, E. Sakagawa, S. Ohya, N. Gotoh, H. Tsujimoto, T. Nishino, Substrate specificities of MexAB-OprM, MexCD-OprJ, and MexXY-oprM efflux pumps in *Pseudomonas aeruginosa*, Antimicrob. Agents Chemother. 44 (12) (2000) 3322–3327.

[8] H. Maseda, H. Yoneyama, T. Nakae, Assignment of the substrate-selective subunits of the MexEF-OprN multidrug efflux pump of *Pseudomonas aeruginosa*, Antimicrob. Agents Chemother. 44 (3) (2000) 658–664.

[9] S.R. Morshed, Y. Lei, H. Yoneyama, T. Nakae, Expression of genes associated with antibiotic extrusion in *Pseudomonas aeruginosa*, Biochem. Biophys. Res. Commun. 210 (2) (1995) 356–362.

[10] A. Lee, W. Mao, M.S. Warren, A. Mistry, K. Hoshino, R. Okumura, H. Ishida, O. Lomovskaya, Interplay between efflux pumps may provide either additive or multiplicative effects on drug resistance, J. Bacteriol. 182 (11) (2000) 3142–3150.

[11] M. Germ, E. Yoshihara, H. Yoneyama, T. Nakae, Interplay between the efflux pump and the outer membrane permeability barrier in fluorescent dye accumulation in *Pseudomonas aeruginosa*, Biochem. Biophys. Res. Commun. 261 (2) (1999) 452–455.

[12] For review: T. Nakae, Role of membrane permeability in determining antibiotic resistance in *Pseudomonas aeruginosa*, Microbiol. Immunol. 39 (4) (1995) 221–229, and reference therein.

[13] O. Lomovskaya, M.S. Warren, A. Lee, J. Galazzo, R. Fronko, M. Lee, J. Blais, D. Cho, S. Chamberland, T. Renau, R. Leger, S. Hecker, W. Watkins, K. Hoshino, H. Ishida, V.J. Lee, Identification and characterization of inhibitors of multidrug resistance efflux pumps in *Pseudomonas aeruginosa* : novel agents for combination therapy, Antimicrob. Agents Chemother. 45 (1) (2001) 105–116.

[14] P.G. Mortimer, L.J. Piddock, A comparison of methods used for measuring the accumulation of quinolones by Enterobacteriaceae, *Pseudomonas aeruginosa* and *Staphylococcus aureus*, J. Antimicrob. Chemother. 28 (5) (1991) 639–653.

[15] For review: W.P. Ambrose, P.M. Goodwin, J.H. Jett, A.V. Orden, J.H. Werner, R.A. Keller, Single-molecule fluorescence spectroscopy at ambient temperature, Chem. Rev. 99 (10) (1999) 2929–2956.

[16] For review: S. Weiss, Fluorescence Spectroscopy of single biomolecules, Science 283 (1999) 1676–1683.

[17] For book: C. Zander, R. Keller, J. Enderlein, Single-Molecule Detection in Solution: Methods and Applications, Wiley, New York, 2002.

[18] T. Schmidt, G. Schutz, W. Baumgartner, H. Gruber, H. Schindler, Imaging of single-molecule diffusion, Proc. Natl. Acad. Sci. USA 93 (1996) 2926–2929.

[19] R.A. Keller, W.P. Ambrose, P.M. Goodwin, J.H. Jett, J.C. Martin, M. Wu, Single-molecule fluorescence analysis in solution, Appl. Spectrosc. 50 (1996) 12A–32A.

[20] S. Nie, D.T. Chiu, R.N. Zare, Probing individual molecules with confocal fluorescence microscopy, Science 266 (1994) 1018–1021.

[21] X.-H. Xu, E.S. Yeung, Long-range electrostatic trapping of single protein molecules at a liquid/solid interface, Science 281 (1998) 1650–1653.

[22] X.-H. Xu, E.S. Yeung, Direct measurement of single-molecule diffusion and photodecomposition in free solution, Science 275 (1997) 1106–1109.

[23] X.-H.N. Xu, R. Jeffers, J. Gao, B. Logan, Novel solution-phase immunoassays for molecular analysis of tumor markers, Analyst 126 (2001) 1285–1292.
[24] T.A. Byassee, W.C. Chan, S. Nie, Probing single molecules in single living cells, Anal. Chem. 72 (2000) 5606–5611.
[25] Y. Sako, S. Minoghchi, T. Yanagida, Single-molecule imaging of EGFR signalling on the surface of living cells, Nat. Cell Biol. 2 (2000) 168–172.
[26] M. Ueda, Y. Sako, T. Tanaka, P. Devreotes, T. Yanagida, Single-molecule analysis of chemotactic signaling in Dictyostelium cells, Science 294 (2001) 864–867.
[27] A. Ocaktan, H. Yoneyama, T. Nakae, Use of fluorescence probes to monitor function of the subunit proteins of the MexA-MexB-OprM drug extrusion machinery in *Pseudomonas aeruginosa*, J. Biol. Chem. 272 (35) (1997) 21964–21969.
[28] H. Yoneyama, H. Maseda, H. Kamiguchi, T. Nakae, Function of the membrane fusion protein MexA of the MexAB-OprM efflux pump in *Pseudomonas aeruginosa* without an anchoring membrane, J. Biol. Chem. 275 (7) (2000) 4628–4634.
[29] S.V. Kyriacou, M.E. Nowak, W.J. Brownlow, X.-H.N. Xu, Single live cell imaging for real-time monitoring of resistance mechanism in *Pseudomonas aeruginosa*, J. Biomed. Opt. 7 (4) (2002) 576–586.
[30] X.-H.N. Xu, Q. Wan, S. Kyriacou, W. Brownlow, M. Nowak, Use single live cell imaging and fluorescence spectroscopy for direct observation of substrate induction of resistance mechanism in *Pseudomonas aeruginosa*, (submitted).
[31] X.-H.N. Xu, J. Chen, R. Jeffers, S. Kyriacou, Direct measurement of sizes and dynamics of single living membrane transporters using nano-optics, Nano Lett. 2 (2002) 175–182.
[32] C.K. Stover, X.Q. Pham, A.L. Erwin, S.D. Mizoguchi, P. Warrener, M.J. Hickey, F.S. Brinkman, W.O. Hufnagle, D.J. Kowalik, M. Lagrou, R.L. Garber, L. Goltry, E. Tolentino, S. Westbrock-Wadman, Y. Yuan, L.L. Brody, S.N. Coulter, K.R. Folger, A. Kas, K. Larbig, R. Lim, K. Smith, D. Spencer, G.K. Wong, Z. Wu, I.T. Paulsen, Complete genome sequences of *Pseudomonas aeruginosa* PA01, an opportunistic pathogen, Nature 406 (2000) 959–964.